ADVANCES IN ATMOSPHERIC SCIENCES, VOL. 23, NO. 1, 2006, 141–148

A Note on the Relationship Between Temperature and Water Vapor over Oceans, Including Sea Surface Temperature Effects

C.-L. SHIE*[1,2], W.-K. TAO[2], and J. SIMPSON[2]

[1] *Goddard Earth Sciences and Technology Center, University of Maryland, Baltimore County, Baltimore, Maryland* 21250, *USA*

[2] *Laboratory for Atmospheres, NASA Goddard Space Flight Center, Greenbelt, Maryland* 20771, *USA*

(Received 25 February 2005; revised 26 September 2005)

ABSTRACT

An ideal and simple formulation is successfully derived that well represents a quasi-linear relationship found between the domain-averaged water vapor, Q (mm), and temperature, T (K), fields for the three tropical oceans (i.e., the Pacific, Atlantic and Indian Oceans) based on eleven GEOS-3 [Goddard Earth Observing System (EOS) Version-3] global re-analysis monthly products. A $Q-T$ distribution analysis is also performed for the tropical and extra-tropical regions based on *in-situ* sounding data and numerical simulations [GEOS-3 and the Goddard Cumulus Ensemble (GCE) model]. A similar positively correlated $Q-T$ distribution is found over the entire oceanic and tropical regions; however, Q increases faster with T for the former region. It is suspected that the tropical oceans may possess a moister boundary layer than the Tropics. The oceanic regime falls within the lower bound of the tropical regime embedded in a global, curvilinear $Q-T$ relationship. A positive correlation is also found between T and sea surface temperature (SST); however, for one degree of increase in T, SST is found to increase 1.1 degrees for a warmer ocean, which is slightly less than an increase of 1.25 degrees for a colder ocean. This seemingly indicates that more (less) heat is needed for an open ocean to maintain an air mass above it with a same degree of temperature rise during a colder (warmer) season [or in a colder (warmer) region]. Q and SST are also found to be positively correlated. Relative humidity (RH) exhibits similar behaviors for oceanic and tropical regions. RH increases with increasing SST and T over oceans, while it increases with increasing T in the Tropics. RH, however, decreases with increasing temperature in the extratropics. It is suspected that the tropical and oceanic regions may possess a moister local boundary layer than the extratropics so that a faster moisture increase than a saturated moisture increase is favored for the former regions. T, Q, saturated water vapor, RH, and SST are also examined with regard to the warm and cold "seasons" over individual oceans. The Indian Ocean warm season dominates in each of the five quantities, while the Atlantic Ocean cold season has the lowest values in most categories. The higher values for the Indian Ocean may be due to its relatively high percentage of tropical coverage compared to the other two oceans. However, Q is found to increase faster for colder months from individual oceans, which differs from the general finding in the global $Q-T$ relationship that Q increases slower for a colder climate. The modified relationship may be attributed to a possible seasonal (warm and cold) variability in boundary layer depth over oceans, or to the small sample size used in each individual oceanic group.

Key words: moisture temperature relationship, quasi-equilibrium states, Tropics, oceans

1. Introduction

In recent years, cloud-resolving models (CRMs) have been used as a sophisticated and flexible numerical tool to study the role of clouds in the energy and hydrological cycles (as well as the numerically-generated quasi-equilibrium thermodynamic states) in the tropical radiative-convective system (e.g., Islam et al., 1993; Held et al., 1993; Tao and Simpson, 1993; Randall et al. 1994; Sui et al., 1994; Grabowski et al., 1996; Robe and Emanuel, 1996; Tao et al., 1999; Wu and Moncrieff, 1999; Xu and Randall, 1999; Tao et al., 2001; Shie et al., 2003; and others). Among these studies [see the brief summaries in Tao et al. (1999)

*E-mail: shie@agnes.gsfc.nasa.gov

and Shie et al. (2003)], two distinct two-dimensional (2D) CRM simulations produced by Sui et al. (1994) and Grabowski et al. (1996) showed considerably different quasi-equilibrium states. In an attempt to resolve such a significant numerical finding, a series of systematic numerical studies were recently performed (Tao et al., 1999, 2001; and Shie et al., 2003) over a tropical oceanic domain using the 2D Goddard Cumulus Ensemble (GCE) model with imposed initial conditions taken from the 1956 Marshall Islands Experiment [originally used in Sui et al. (1994) and Grabowski et al. (1996)]. The plausible dynamical and physical causes that accounted for such a significant discrepancy in the modeled quasi-equilibrium state were genuinely identified and elaborated on in these studies [Tao et al. (1999) and Shie et al. (2003)]. One striking feature that emerged as a result was a quasi-linear relationship between domain-averaged temperature, T (K) and water vapor, Q (mm). In these earlier studies [Tao et al. (1999) and Shie et al. (2003)], the forced maintenance of two different wind profiles was found to be dynamically critical in determining the various tropical quasi-equilibrium states.

Stephens (1990) found a positive correlation between monthly mean precipitable water and sea surface temperature by using 52 months of precipitable water from passive microwave radio and National Meteorological Center (NMC) global gridded SST dataset blended with *in-situ* and satellite observations. It also showed that such analyses based on global or regional scale resulted in differences in both phase and amplitude that could be used as a tracer of large-scale circulation. The purpose of the present study is, therefore, to extend an investigation on the water and energy cycles into three major tropical oceans, i.e., the Pacific, Atlantic and Indian Oceans, for relatively "warm/moist" and "cold/dry" regimes. The basic goals of this note are simply to clarify (1) whether the water vapor-temperature or relative humidity-temperature relations for the respective oceanic regions would resemble or differ from those found in the Tropics, (2) and what the impact sea surface temperature (SST) may have on those relations found over oceans. The correlated SST signature and large-scale circulation suggested in Stephens (1990) is a feature that will not be examined in this study. We, however, extend the targeted area of this study on the water vapor-temperature and relative humidity-temperature relations from the tropical and oceanic regions to the extratropical regions. The related findings are also presented.

The GEOS-3 [Goddard Earth Observing System (EOS) Version-3] global re-analysis monthly products (Hou et al., 2001), the GCE simulated experiments, as well as observations from the field experiments are described in section 2. Section 3 presents a detailed derivation of the idealized theoretical relations representing the slopes of the domain-averaged water vapor and temperature distributions. These theoretical relations are ideally obtained based on a thermodynamic concept. Section 4 presents the major findings for the oceanic regions, along with a comparison with the findings for the tropical and extratropical regions. A final remark is given in section 5.

2. Data

There are eleven monthly GEOS-3 global reanalysis datasets used in this study to obtain the temperature, water vapor, and SST fields for the three targeted oceanic regions, i.e., the Pacific, Atlantic, and Indian Oceans. These monthly-averaged GEOS-3 re-analysis datasets include (1) seven "summer" months—May, June, July and August in 1998 for SCSMEX (the 1998 South China Sea Monsoon Experiment, Lau et al., 2000) and July, August and September in 1999 for KWAJEX (the 1999 Kwajalein Atoll field experiment, Yuter et al., 2004), and (2) four "winter" months—January, February, November, and December in 1998. The GEOS-3 "summer" months were intended to match the SCSMEX and KWAJEX periods, while the "winter" months were chosen for the same year as SCSMEX, namely 1998. The GEOS-3 seven "summer" and four "winter" months are sorted into three oceanic regions approximating the "Pacific" (22°S– 22°N, 120°E–120°W), "Atlantic" (22°S–22°N, 65°W–15°W), and "Indian" (22°S–10°N, 40°E–110°E) Oceans, respectively.

The moisture and temperature fields representing the global region, i.e., the Tropics and extratropics (shown later in Fig. 2) are based on three data resources: (1) a series of tropical (Marshall Island) numerical simulations produced by the GCE model (e.g., Tao et al. 1999, 2001, and Shie et al., 2003), (2) tropical sounding observations from *in-situ* or field experiment sites such as Marshall Island, SCSMEX, KWAJEX, TOGA-COARE (Tropical Ocean and Global Atmosphere Coupled Ocean-Atmosphere Response Experiment, Webster and Lukas, 1992), and GATE (Global Atmospheric Research Programme Atlantic Experiment, Houze and Betts, 1981), and (3) the aforementioned GEOS-3 global re-analysis products that are also applied for both tropical and extratropical regions. Note that the "tropical" data referred to here include the GCE model simulations, the sounding observations, and the GEOS-3 data attained from the two latitudinal bands (0°–30°N and 0°–30°S), while the "extratropical" data include the GEOS-3 data obtained from the four latitudinal bands, viz. "mid-latitudes": 30°–60°N and 30°–60°S; "high-latitudes": 60°–90°N and 60°–90°S.

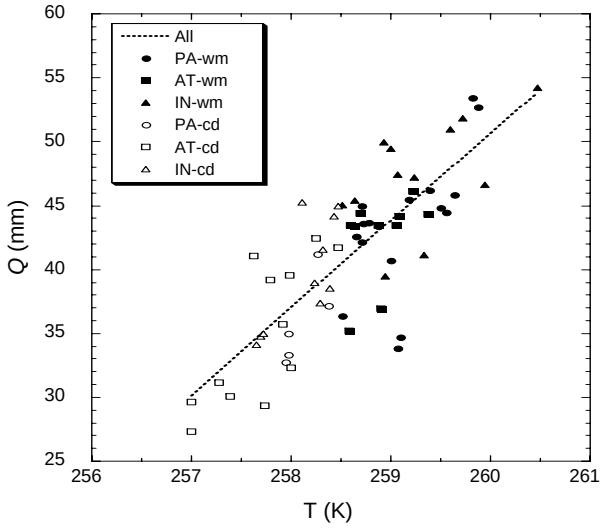

Fig. 1. Scatter diagram of domain-averaged water vapor versus temperature for three oceanic regions— "Atlantic" (22°S–22°N, 65°–15°W), "Indian" (22°S–10°N, 40°E–110°E) and "Pacific" Ocean (22°S–22°N, 120°E–120°W)—in "warm" (denoted as "wm") and "cold" (denoted as "cd") months. The relatively warm and cold regimes are divided based on a criterion temperature of 258.5 K. A regression line (dotted line) with a slope of 6.8 mm K^{-1} obtained by applying a linear regression method to the group including all data points is also shown.

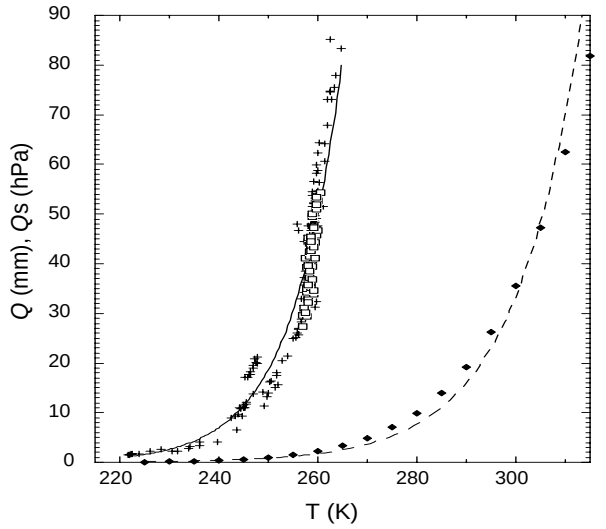

Fig. 2. The oceanic domain-averaged water vapor (mm)-temperature (K) (also shown in Fig. 1) (open squares), along with the curvilinear distribution of domain-averaged water vapor-temperature for 135 data points from global regions (crosses and solid curve) and the curvilinear distribution of saturated water vapor pressure (hPa)-temperature obtained based on the Clausius-Clapeyron equation (diamonds and dashed curve). The curvilinear lines are obtained using an exponential fitting.

3. Idealized formulation

Horizontal integration (average) of the equations for potential temperature (θ) and water vapor (mixing ratio, $q_{\rm v}$) over the model domain yields

$$c_p\frac{\partial\bar{T}}{\partial t} = [L_{\rm v}(\bar{c}-\bar{e}) + L_{\rm s}(\bar{d}-\bar{s}) + L_{\rm f}(\bar{f}-\bar{m})] - c_p\overline{\pi w}\frac{\partial\bar{\theta}}{\partial z} - c_p\bar{\pi}\frac{1}{\bar{\rho}}\frac{\partial}{\partial z}\bar{\rho}\overline{w'\theta'} + \overline{Q_R}\,, \quad (1)$$

and

$$L_{\rm v}\frac{\partial\bar{q}_{\rm v}}{\partial t} = -\,[L_{\rm v}(\bar{c}-\bar{e}) + L_{\rm s}(\bar{d}-\bar{s})] - L_{\rm v}\bar{w}\frac{\partial\bar{q}_{\rm v}}{\partial z} - L_{\rm v}\frac{1}{\bar{\rho}}\frac{\partial}{\partial z}\bar{\rho}\overline{w'q'_{\rm v}}\,, \quad (2)$$

where variables with an overbar are horizontally-averaged quantities, and deviations from the means are denoted by a prime, while c, e, d, s, f and m are condensation, evaporation, deposition, sublimation, freezing, and melting, respectively. T is temperature, and $\bar{\pi} = (p/p_{00})^{R/c_p}$ is the nondimensional pressure, where p is the dimensional pressure and p_{00} the reference pressure taken to be 1000 hPa. c_p is the specific heat of dry air at constant pressure, and R is the gas constant for dry air. $-\bar{w}(\partial\bar{\theta}/\partial z)$ and $-\bar{w}(\partial\bar{q}_{\rm v}/\partial z)$ are the mean advection of potential temperature (cooling) and water vapor (moistening); $\bar{w}$ is the prescribed large-scale mean vertical velocity (constant with time); $\partial\bar{\theta}/\partial z$ and $\partial\bar{q}_{\rm v}/\partial z$ are the model mean vertical potential temperature and water vapor gradients (varying with time); $(-1/\rho)[\partial(\bar{\rho}\overline{w'\theta'})/\partial z]$ and $(-1/\rho)[\partial(\bar{\rho}\overline{w'q'_{\rm v}})/\partial z]$ are the vertical eddy flux convergence/divergence for potential temperature and water vapor, respectively. Q_R is the radiative heating containing solar and infrared radiation. The variables $L_{\rm v}, L_{\rm f}$, and $L_{\rm s}$ are the latent heats of condensation, fusion and sublimation, respectively. For an equilibrium state, the vertically integrated Eqs. (1) and (2) can be reduced to

$$c_p\frac{\partial[\bar{T}]}{\partial t} = 0\,, \quad (3)$$

and

$$L_{\rm v}\frac{\partial\{\bar{q}_{\rm v}\}}{\partial t} = 0\,, \quad (4)$$

where $[\bar{T}]$ and $\{\bar{q}_{\rm v}\}$ are the domain-averaged and density-weighted temperature (K), and the vertically integrated column water vapor (mm) (the so called "precipitable water"), respectively. The units for $\{\bar{q}_{\rm v}\}$ are in mm since $\bar{q}_{\rm v}$ (g kg^{-1}) has been integrated along a vertical column with the vertical scale height becoming implicit. Curly parentheses are thus used to denote such a vertical integral for water vapor to distinguish them from the brackets that represent a vertical average for temperature (along with an explicit vertical scale height). The vertically integrated static energy

densities (J m^{-2}) due to the domain-averaged temperature and water vapor, respectively, at an occurred equilibrium state, which depend on τ that represents various equilibrium states, can then be represented as follows:

$$C_1(\tau) = c_p \tilde{\bar{\rho}}_{air}[\bar{T}]H \ , \quad (5)$$

$$C_2(\tau) = L_v \tilde{\bar{\rho}}_w\{\bar{q}_v\} \quad (6)$$

where $\tilde{\bar{\rho}}_{air}$ and $\tilde{\bar{\rho}}_w$ are the domain-averaged air and water vapor densities, and H is the vertical scale height of the free atmosphere. By taking the derivative of Eq. (6) over Eq. (5) and assuming that $\tilde{\bar{\rho}}_{air}$ and $\tilde{\bar{\rho}}_w$ are invariant with various quasi-equilibrium states, and that the derivative change of L_v with temperature is negligible, a theoretical relationship between the variations of water vapor and temperature with respect to the quasi-equilibrium state can then be obtained as follows:

$$\frac{d\{\bar{q}_v\}}{d[\bar{T}]} = (c_p \tilde{\bar{\rho}}_{air} H / L_v \tilde{\bar{\rho}}_w)\frac{dC_2}{dC_1}(\tau) \ . \quad (7)$$

By assuming that $\tilde{\bar{\rho}}_w$ and $\tilde{\bar{\rho}}_{air}$ are 10^3 and 1 kg m^{-3}, respectively, and that H is 10 km, Eq. (7) can be further simplified as

$$\frac{d\{\bar{q}_v\}}{d[\bar{T}]} = C_{ideal}\frac{dC_2}{dC_1}(\tau) \ , \quad (8)$$

where $C_{ideal} = (c_p/L_v)$ (10^4 mm) which increases from 4.016 (mm K^{-1}) to 4.462 (mm K^{-1}) as L_v decreases from 2.5×10^6 J kg^{-1} (at 0°C) to 2.25×10^6 J kg^{-1} (at 100°C) at a c_p of 1004 J K^{-1} kg^{-1}. Eq. (8) provides a simplified theoretical relationship for the derivative of $\{\bar{q}_v\}$ and $[\bar{T}]$ that depends on a near constant C_{ideal} [e.g., 4.239 mm K^{-1}, a mean of 4.016 mm K^{-1} and 4.462 mm K^{-1}] and a varied dC_2/dC_1. Physically, dC_2/dC_1 can be considered as a ratio of the static energy (contribution) change due to temperature (C_1) and moisture (C_2), respectively, as the equilibrium state τ varies. The special regime where dC_2/dC_1 equals unity implies that both temperature and moisture contribute to the static energy at the same rate for different equilibrium states τ (i.e., C_1 and C_2 may only differ by a pure constant as τ changes). Under such an "ideal" condition, the slope of $(\{\bar{q}_v\}, [\bar{T}])$ in Eq. (8) can be reduced to C_{ideal}. The GCE-modeled "tropical" regime is found close to such an ideal regime (see details later in the next section). Generally speaking, the moisture-temperature slope is proportional to the derivative of static energy contributions (dC_2/dC_1) by a factor of C_{ideal}.

4. Results

The domain-averaged water vapor versus temperature obtained from eleven months of GEOS-3 data for three oceanic regions—"Atlantic" (22°S–22°N, 65°W–15°W), "Indian" (22°S–10°N, 40°E–110°E) and "Pacific" Oceans (22°S–22°N, 120°E–120°W) are shown in Fig. 1. Each oceanic group is divided into "warm" and "cold" regimes based on a criterion air temperature of 258.5 K that is near an averaged temperature including all the oceanic data examined. A linear regression method has also been applied to the entire data group shown in Fig. 1 to obtain a regression line. A positive water vapor-temperature correlation, i.e., a dC_2/dC_1 value of 1.60, is obtained based on the regression line consisting of data from all three oceanic groups (Fig. 1, the regression line is not shown). The domain-averaged moisture-temperature data obtained from the global regions (i.e., a total of 135 data points collected for the Tropics and mid and, high latitudes that are described in section 2) are also included here and drawn together with the oceanic moisture-temperature data (shown in Fig. 1) in Fig. 2. Figure 2 shows that the oceanic moisture-temperature data (i.e., 27–55 mm/257–260.5 K denoted as open squares) reside within the lower bound of the tropical moisture/temperature range (i.e., 30–86 mm/255–265 K). The oceanic data (a dC_2/dC_1 value of 1.60) show a steeper slope relative to the tropical regions [e.g., a dC_2/dC_1 value of 1.318 within the regime of 30–86 mm/255–265 K including all the tropical data, or a dC_2/dC_1 value of 0.995 (near unity) within the regime of 46–83 mm/256–265 K containing only the GCE-modeled tropical simulations] that are embedded in the global data (crosses) with a curvilinear distribution (the curve on the left hand side). The steeper slope found over oceans implies that the overall oceanic regions favor a quicker increase in water vapor with increasing temperature than the Tropics do. The faster increase of moisture (with increased temperature) in the oceanic region than the tropical region may be due to a possibly moister local boundary layer in the tropical oceans than in the Tropics.

The curvilinear moisture-temperature distribution for the global regions bears a remarkable resemblance to the famous Clausius-Clapeyron curve of saturated water vapor pressure (hPa)-temperature (dark diamonds and the thick dashed line on the right hand side in Fig. 2). This interesting feature seemingly indicates that a fundamental thermodynamic theory may be generally implied in various scales of scenarios ranging from a micro to a macro scale. Our earlier model works (Tao et al., 1999 and Shie et al., 2003) showed that the forced maintenance of two different wind profiles in the Tropics led to two different equilibrium states, which held a locally quasi-linear moisture-temperature relationship that is now found embedded in a globally curvilinear distribution in this study. Such a genuine finding (a commonly found curvilinear moisture-temperature relationship for both micro and macro

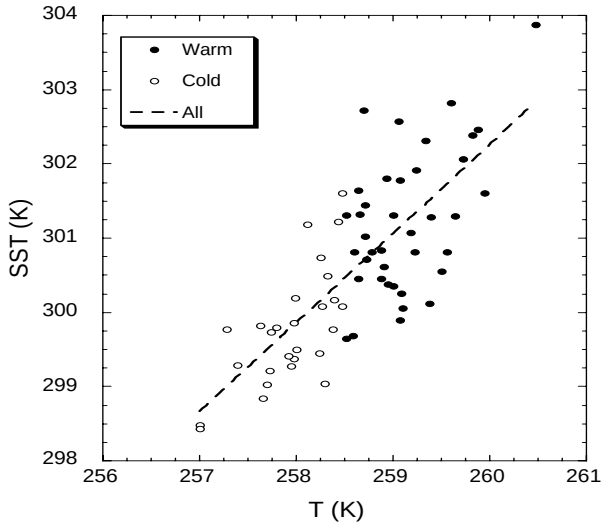

Fig. 3. Scatter diagram of domain-averaged SST versus temperature for the six "seasonal" ocean groups (same as those in Fig. 1) with the open and closed circles denoting data from the "cold" and "warm" months, respectively. A regression line with a slope of 1.2 K K^{-1} obtained by applying a linear regression method to the group including all data points is also shown.

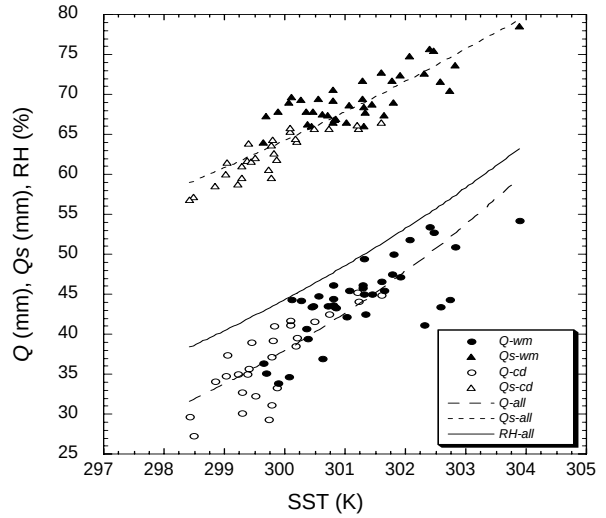

Fig. 4. The distribution of domain-averaged water vapor and saturated water vapor (mm) versus SST (K) for the six "seasonal" ocean groups (same as those in Fig. 1) with the closed and open circles (triangles) denoting water vapor (saturated water vapor) from the warm and cold months, respectively. The respective curvilinear lines are obtained including all the water vapor (long-dashed line) and saturated water vapor (short-dashed line) data points using an exponential regression fitting. A regression line obtained by including all the relative humidity (%) data points is also shown (solid line). The individual relative humidity data points are not shown here for the sake of figure clarity.

scales) may suggest that the dynamics are crucial to the climate, while the thermodynamics are equally important to play a role of adjustment in the hydrological cycle. Nonetheless, an extensive study may be necessary to further confirm the scientific insight behind such a resemblance. Note that the dC_2/dC_1 values for the six individual "seasonal" oceanic groups (the corresponding regression lines are not shown in Fig. 1), however, distinguish between "warm and cold seasons", i.e., warm months have smaller values (0.98, 1.32, and 1.76), while cold months tend to have larger values (2.16, 2.35, and 3.23). This implies that water vapor increases faster (slower) for colder (warmer) oceanic climate, which apparently differs from what has been generally found in the curvilinear moisture-temperature relationship (Fig. 2) that water vapor increases slower (faster) for colder (warmer) climate. It is suspected that such a modified relation for the ocean regions may be related (or attributed) to a possible seasonal (warm and cold) variability in boundary layer depth over oceans, i.e., the boundary layer over a colder oceanic region tends to be shallower than that over a warmer ocean. We also suspect that the correlated "vertically integrated water vapor" and "density-weighted temperature" may be more representative of the boundary layer than the free troposphere based on the fact that in the troposphere water vapor decreases exponentially with height while the temperature decreases with a linear lapse rate. As such, the variation of boundary layer depth may indeed play a critical role in modifying the moisture-temperature relations. Or, this modified moisture-temperature relation is possibly due to the small sample size used in each individual oceanic group (i.e., seven and four months for summer and winter, respectively). This demands a future extensive study using a larger data population to confirm the results one way or the other.

As mentioned in the introduction, a positive correlation was found between monthly mean precipitable water and sea surface temperature based on 52 months of precipitable water from passive microwave radio and NMC blended SST (Stephens, 1990). A similar feature is also found in this note, yet with less data samples (i.e., 11 months used here versus 52 months). The corresponding domain-averaged SST versus temperature obtained from GEOS-3 for the six "seasonal" ocean groups are shown in Fig. 3 with the open and dark circles denoting data from the "warm" and "cold" months, respectively. Similar to the positively correlated moisture and temperature shown in Fig. 1, SST also generally increases with increasing temperature (T). A positive correlation is also found between T and SST. Based on the slope value obtained for the regression line (dashed line in Fig. 3), there is about

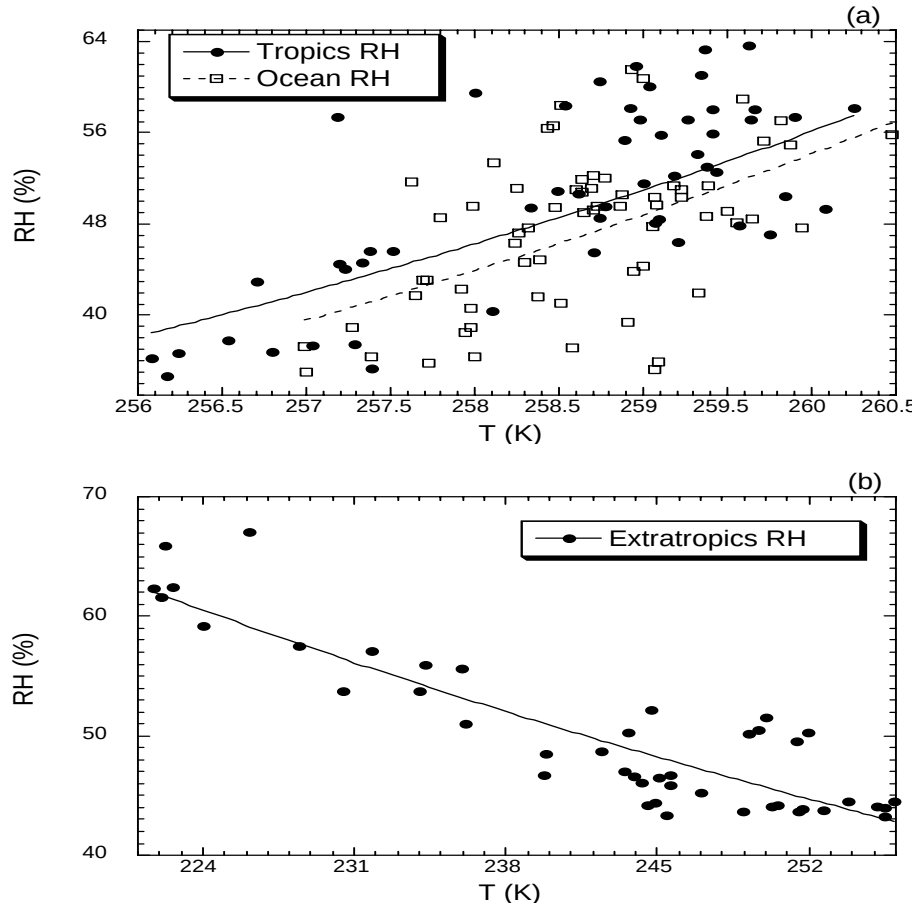

Fig. 5. The distribution of domain-averaged relative humidity (%) versus temperature (K) for (a) the tropical (closed circles and solid line) and oceanic regions (open squares and dashed line), and (b) extratropical regions using the GEOS-3 data. The curvilinear lines are obtained using an exponential fitting.

1.2 degrees of SST change for one degree of temperature change; however, SST changes slightly less (i.e., 1.1 degrees) for the warm months than for the cold months (i.e., 1.25 degrees) based on the corresponding slopes that are not shown in Fig. 3. This seemingly indicates that more (less) heat is needed for an open ocean to maintain an air mass above it [the ocean] with a same degree of temperature increase during a colder (warmer) season [or in a colder (warmer) region]. Again, more data samples will be necessary in a future study to further confirm such an argument.

The domain-averaged water vapor and saturated water vapor (mm) for the six "seasonal" ocean groups are shown versus SST in Fig. 4 with the clsoed and open circles (triangles) denoting water vapor (saturated water vapor) from the warm and cold months, respectively. The respective regression lines are obtained including all the water vapor (long-dashed line) and saturated water vapor (short-dashed line) data points. Based on the two respective curves shown in Fig. 4, both water vapor and water vapor pressure increase as SST increases, yet the former has a faster rate of increase than the latter, particularly for a higher SST. As such, the corresponding relative humidity fields (i.e., the solid regression curve) are found increasing with SST. Note that the individual relative humidity data points are not shown in Fig. 4 for the sake of figure clarity. The positively correlated water vapor (or precipitable water) and SST shown in Fig. 4 (long-dashed line) quantitatively agree well with the results found in Stephens (1990). Accordingly, water vapor increasing from 32 mm (equivalent to 3.2 g cm^{-1}) at 298.5 K (around 25.3°C) to 54 mm (5.4 g cm^{-1}) at 303 K (around 29.8°C) shown in Fig. 4 resembles an increasing amount of precipitable water from 3.4 g cm^{-1} at 25°C to 5.2 g cm^{-1} at 30°C shown in Fig. 6 of Stephens (1990). Similar patterns shown in Fig. 4 can also be attained by replacing SST with temperature (not shown). For example, relative humidity is also found to increase with temperature due

to a faster rate of increase of moisture than saturated moisture as temperature increases.

Figure 5 shows the relative humidity (RH) field for the tropical and extra-tropical regions (based on the GEOS-3 data), along with the oceanic RH discussed above. Relative humidity is found to change with temperature in an interesting two-branch pattern. In one branch (Fig. 5a), RH for the tropical region, viz., 30°S–30°N (dark circles and solid line), generally increases more rapidly from 34%–37% around 256 K to 56%–64% around 259.5–260 K due to a faster increase of moisture than saturated moisture with increased temperature. Relative humidity in the oceanic regions (open squares and dashed line in Fig. 5a) shows a similar pattern of positively correlated RH-T (as also mentioned earlier), but generally with a lower RH magnitude than that in the tropical region. This similar pattern found between the tropical and oceanic regions may be due to the fact that three oceans occupy most of the Tropics, while the lower RH in the oceanic regions may be attributed to the relatively higher temperature in the oceanic region than in the tropical region (shown in both Fig. 5a and Fig. 2). In the other branch (Fig. 5b), RH for the extratropical regions, viz., 30°–90°N and 30°–90°S is found to decrease much slower (compared to Fig. 5a) from 61–66% around 221 K to 43%–45% around 255–256 K due to a slower increase of moisture than saturated moisture with increasing temperature. Apparently, the faster (slower) increase of moisture than saturated moisture with increasing temperature for the tropical-oceanic (extratropical) regions accounts for the increasing (decreasing) RH with increased temperature for the respective regions. We suspect that a possibly moister boundary layer in the tropical-oceanic region than in the extratropics may favor the former region to have a faster increase of moisture as temperature increases.

5. Concluding remarks

By applying eleven months of GEOS-3 data to three oceanic regions—the Atlantic, Indian and Pacific Oceans—an overall positively correlated moisture-temperature distribution is found located near the lower bound of the tropical regime embedded in a globally curvilinear moisture-temperature relationship (Fig. 2). The overall oceanic regime, however, has a steeper slope (i.e., a larger dC_2/dC_1 value) than the Tropics that implies a quicker increase in water vapor with increasing temperature over the oceans. It is suspected that the tropical oceans may possess a more humid boundary layer than the Tropics. As expected, the air temperature over the oceans is found to increase with increasing SST; however, for one degree of temperature increase, they need a slightly smaller increase in SST for a warmer ocean (viz., 1.1 degrees of increase) as compared to a colder ocean (viz., 1.25 degrees of increase). This seemingly suggests that more (less) heat may be needed for an open ocean during a colder (warmer) season [or in a colder (warmer) region] to maintain an air mass with the same degree of temperature rise. A positive correlation between moisture and SST is also found, which quantitatively resembles the results found in Stephens (1990) even though the sample size used in this study is about one order of magnitude smaller than that in Stephens (1990). Relative humidity is another quantity that bears similar features in the oceanic and tropical regions, respectively. Accordingly, RH increases with increasing SST, as well as the temperature over the oceans, as it also increases with increasing temperature in the Tropics. Relative humidity was, however, found to decrease with increasing temperature for mid and high latitudes. The increasing (decreasing) RH with increasing temperature for the tropical-oceanic (extra tropical) regions is attributed to the faster (slower) increase of moisture than saturated moisture with increased temperature for the respective regions. The tropical and oceanic regions may possess a moister local boundary layer than the extratropics so that a faster moisture increase is favored for the former regions.

The domain-averaged temperature, water vapor, saturated water vapor, relative humidity, and sea surface temperature are also briefly examined for the respective "seasons" (i.e., warm and cold months) and oceans (i.e., Pacific, Atlantic, and Indian Oceans). The "warm" Indian Ocean is found leading in each of the five studied quantities, while the "cold" Atlantic trails in most categories. The dominance by the Indian Ocean may be due to its relatively high percentage of tropical coverage compared to its other two counterpart oceans. As the moisture-temperature distributions are examined with their respective warm and cold months, it is found that water vapor increases faster (slower) for colder (warmer) climate, which differs from the general finding shown in the curvilinear moisture-temperature relationship (Fig. 2) in which water vapor increases slower (faster) for colder (warmer) climate. Such modified relationships may be primarily attributed to the small sample size used in each individual oceanic group, or to a possible oceanic impact. As for the oceanic impact, it is suspected that a possible seasonal (warm and cold) variability in boundary layer depth over the oceans, i.e., a shallower (deeper) boundary layer over a colder (warmer) oceanic region, may indeed play a critical role in modifying the moisture-temperature relation. Accordingly, such a $Q-T$ relation may be more representative of the boundary layer than the free troposphere since, in the troposphere, water vapor decreases exponentially with height while the temperature decreases with a linear

lapse rate. Nonetheless, the aforementioned features involving the individual oceans may not be conclusive until an extensive data population is included and analyzed in the future. Moreover, we suspect that the relative contribution to the energy-water vapor budget from thermodynamics and dynamics may very likely differ between the boundary layer and the free troposphere, i.e., dynamics may be more important than thermodynamics in the free troposphere, while thermodynamics may possibly overwhelm the dynamics in the boundary layer in establishing the moisture-temperature relationship. To continue and extend the water and temperature vertical distribution analysis, a study (using an extensive data population) of the boundary layer and free troposphere, respectively, is therefore planned. It is also hoped that through this future study we may be able to consolidate the scientific insight originating from the remarkable resemblance of the curvilinear moisture-temperature distribution for the global regions to the famous Clausius-Clapeyron curve presented in this note.

Acknowledgments. The authors wish to thank Dr. A. Hou and Ms. S. Zhang for kindly providing us their GEOS-3 global reanalysis temperature, water vapor, and sea surface temperature fields. This study was supported by the NASA Headquarters Physical Climate Program and by the NASA TRMM project. The authors are also grateful to Dr. R. Kakar (NASA/HQ) for his support of this research. Acknowledgment is also made to NASA/Goddard Space Flight Center for computer time used in the research.

REFERENCES

Grabowski, W. W., M. W. Moncrieff, and J. T. Kiehl, 1996: Long-term behavior of precipitating tropical cloud systems: A numerical study. *Quart. J. Roy. Meteor. Soc.*, **122**, 1019–1042.

Held, I. M., R. S. Hemler, and V. Ramaswamy, 1993: Radiative-convective equilibrium with explicit two-dimensional moist convection. *J. Atmos. Sci.*, **50**, 3909–3927.

Hou, A. Y., S. Zhang, A. da Silva, W. Olson, C. Kummerow, and J. Simpson, 2001: Improving global analysis and short-range forecast using rainfall and moisture observations derived from TRMM and SSM/I passive microwave sensors. *Bull. Amer. Meteor. Soc.*, **81**, 659–679.

Islam, S., R. L. Bras, and K. A. Emanuel, 1993: Predictability of mesoscale rainfall in the Tropics. *J. Appl. Meteor.*, **32**, 297–310.

Lau, K. M., and Coautors, 2000: A report of the field operations and early results of the South China Sea Monsoon Experiment (SCSMEX). *Bull. Amer. Meteor. Soc.*, **81**, 1261–1270.

Randall, D. A., Q. Hu, K.-M. Xu, and S. K. Krueger, 1994: Radiative-convective disequilibrium. *Atmos. Res.*, **31**, 315–327.

Robe, F. R., and K. A. Emanuel, 1996: Dependence of tropical convection on radiative forcing. *J. Atmos. Sci.*, **53**, 3265–3275.

Shie, C.-L. , W.-K. Tao, J. Simpson, and C.-H. Sui, 2003: Quasi-equilibrium states in the Tropics simulated by a cloud-resolving model. Part 1: Specific features and budget analyses. *J. Climate*, **16**, 817–833.

Stephens, G. L., 1990: On the relationship between water vapor over the oceans and sea surface temperature. *J. Climate*, **3**, 634–645.

Sui, C.-H., K. M. Lau, W.-K. Tao, and J. Simpson, 1994: The tropical water and energy cycles in a cumulus ensemble model. Part I: Equilibrium climate. *J. Atmos. Sci.*, **51**, 711–728.

Tao, W.-K., and J. Simpson, 1993: The Goddard Cumulus Ensemble Model. Part I: Model description. *Terr. Atmos. Oceanic Sci.,* **4**, 35–72.

Tao, W.-K., C.-H. Sui, C.-L. Shie, B. Zhou, K. M. Lau, and M. Moncrieff, 1999: On equilibrium (climate) states simulated by cloud-resolving models. *J. Atmos. Sci.*, **56**, 3128–3139.

Tao, W.-K., C.-L. Shie, and J. Simpson, 2001: Comments on "A sensitivity study of radiative-convective equilibrium in the Tropics with a convection-resolving model". *J. Atmos. Sci.*, **58**, 1328–1333.

Webster, P. J., and R. Lukas, 1992: TOGA COARE: The Coupled Ocean-Atmosphere Response Experiment. *Bull. Amer. Meteor. Soc.*, **73**, 1377–1416.

Wu, X., and M. W. Moncrieff, 1999: Effects of sea surface temperature and large-scale dynamics on the thermodynamic equilibrium state and convection over the tropical western Pacific. *J. Geophys. Res.*, **104**, 6093–6100.

Xu, K.-M., and D. A. Randall, 1999: A sensitivity study of radiative-convective equilibrium in the Tropics with a convection-resolving model. *J. Atmos. Sci.*, **56**, 3385–3399.

Yuter, S., R. A. Houze Jr., E. A. Smith, T. T. Wilheit, E. Zipser, 2004: Physical characterization of tropical oceanic convection observed in KWAJEX. *J. Appl. Meteor*, **44**, 385–415.